Full duplex network access with colorless and source-free optical network units

CICHY Simon* and MASANAS Miquel†
Universitat Politècnica de Catalunya, Enginyeria física
(Dated: May 31, 2019)

In this paper the feasibility of a duplex network based on nested Mach Zehnder modulators is examined as a way to provide colorless and source free ONUs while accessing full bandwidth with neither time interruptions nor Rayleigh backscattering. The analytic framework provided justifies the proposal's attainability, and experimental results sustain the practicality of the proposed downlink data modulation.

I. INTRODUCTION

Passive Optical Networks (PONs) are faced with the tremendous challenge of providing high-speed data services to a multitude of residential users as well as wireless fronthaul and backhaul with a guaranteed Quality of Service in a cost-effective way. Towards meeting this challenge, careful attention should be devoted to the design of the Optical Network Units (ONU), trying to minimize the number of components and avoiding costly and/or sensitive equipment, such as optical sources, while at the same time maintaining performances by the use of high order modulation formats, coherent detection and wavelength diversity. Recent advances in nested Mach Zehnder modulators (n-MZM) with reduced footprint and price hold promise for cost-effective integration into the ONU hardware for the optical IQ modulation of uplink data to be coherently detected at the Optical Line Terminal (OLT).

Here we propose to use a nMZM into the ONU with the dual purpose of both modulating the uplink data and shifting the wavelength of a remotely supplied optical carrier without optical budget penalties due to Rayleigh backscattering. To the hardware, energy and maintenance savings, our proposal adds the benefits of a universal ONU design which is wavelength agnostic and thus eases provision and inventory tasks while allowing for flexible allocation to different Wavelength Division Multiplexing (WDM) channels.

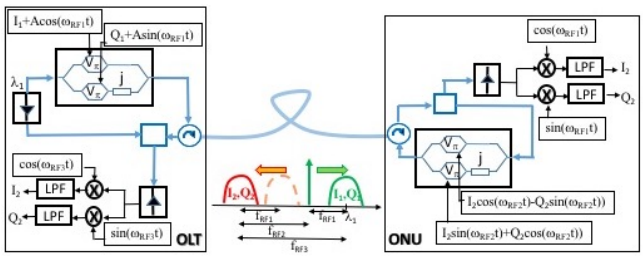

FIG. 1. Global scheme of the proposed system

II. PROPOSAL

Figure 1 shows the basic downlink/uplink optical link configuration of the proposed PON architecture. At the OLT side the I and Q components of the downlink data (I_1, Q_1) are added to RF tones at f_{R1} with a respective 90°phase delay and fed to each of the nested modulators of nMZM biased at their null point. The optical phase difference between nested modulators should be set to 90°. The downlink signal contains the optical IQ downlink data at the wavelength of the OLT laser, λ_1, and a pure tone at $\lambda_1 - f_{Rf1}$ (see green traces in the optical fiber spectrum). This downlink signal is coupled to the fiber link connecting to the ONU through an optical circulator. At the other side of the fiber link, the output of the ONU circulator is split in two to be injected both into a photodetector and into a nMZM. After photodetection, electrical IQ demodulation using multipliers with 90 tones at f_{Rf1} and low pass filtering yields the I and Q downlink data (I_1, Q_1).

At the other splitter output the signal undergoes optical IQ modulation of the uplink data (I_2, Q_2) and wavelength shifting using a combination of 90 relative phase shift tones at the frequency f_{Rf2} into a nMZM. The value f_{Rf2} should be high enough to avoid uplink/downlink carrier and data spectral overlap and prevent power budget shrinkage due to Rayleigh backscattering. The fiber spectrum shows the uplink and downlink spectrum; downlink carrier and data in green, uplink data in red, and useless signal resulting from consecutive modulation of downlink and uplink data and wavelength shifting in dotted orange line. Once the uplink signal arrives at the OLT, and after the optical circulator, it is detected by a tone obtained from the OLT source via null point biasing of a MZM driven by a tone at frequency f_{Rf2}.

In this paper we will expose the idea and the analytical basis of the new system and verify that the data is generated and sent appropriately in a realistic setup, but both the downlink demodulation and the uplink remain to be tested.

* simon.cichy@alu-etsetb.upc.edu
† miquel.masanas@alu-etsetb.upc.edu

III. THEORETICAL BASIS

A. Mathematical fundament

As stated previously this network is based on the usage of nested Mach Zehnder Modulators (nMZM), which use the Pockel's effect on lithium niobate ($LiNbO_3$) crystals to introduce a phase shift linearly dependant on the applied voltage. A single MZM separates the input light beam ideally in 2 equal beams to shift them, but in practice there is an asymmetry that can be accounted for using a parameter κ:

$$E_{MZM} = \frac{E_{in}}{1+\kappa}[e^{j\theta_1(t)} + \kappa e^{j\theta_2(t)}] \tag{1}$$

Where "θ" are the phase shifts $\theta = u\frac{\pi}{V_\pi}$ with "u" the applied voltage. In push-pull configuration $u_1 = -u_2 = \frac{U}{2}$, and the voltage U will be such as $U = V_{Bias} + V_{RF}(t)$.

A nMZM in push pull configuration uses 3 MZM as depicted in the following figure:

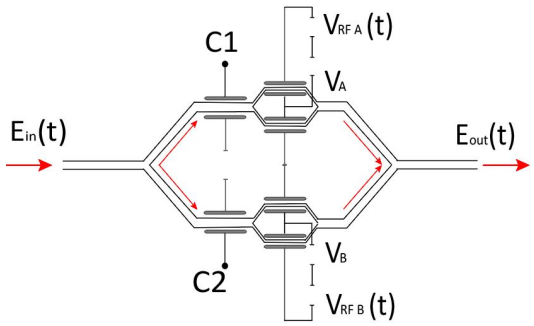

FIG. 2. Schematic view of the applied voltages to a nMZM

The big MZM provides a bias access to each branch via C1 and C2 that allows us to change the optical phase of the two branches. Noting the relevance of phase difference rather than absolute value, we will ground $C_2 = 0$ and without losing generality, the total transfer function will be

$$E_{nMZM} = \frac{E_{in}}{2}\left[\cos\left(\frac{\pi}{2V_\pi}U_A\right) + e^{iC}\cos\left(\frac{\pi}{2V_\pi}U_B\right)\right] \tag{2}$$

In the usual operation, the 2 nested MZM will be biased at their null point and port C1 will be set to provide $\pi/2$ of optical phase difference. Given the push pull operation this assumes in practice equal voltages (at least nominally, and also depending on the intended signs of data modulation and optical phases required for the specific application) in the 3 bias ports.

Linear approximation:
In the intent to anticipate the received data after sending through our setup, we will work on a linear approximation with ideal values. Our goal being to avoid the use of a laser in the ONU, a first nMZM is used to modulate the data on the frequency of the laser and perform a frequency shift at the same time, in order to have a pure tone for the detection. The second nMZM will be used to shift the frequency where the data is modulated, in order to propagate at a different wavelength then the downstream data, and so avoid the negative effect of the backscattering.

For the downlink, considering an input field created by the laser as $E_{in} = e^{j\omega_1 t}$ and the applied tensions to each MZ as in figure 1:

$$\begin{aligned} V_{RFA} &= I_1 + A\cos(\omega_{RF_1}t) \\ V_{RFB} &= Q_1 + A\sin(\omega_{RF_1}t) \end{aligned} \tag{3}$$

with the big MZM set to create a phase difference of j, one obtains the output field:

$$E_{out_1} = e^{j\omega_1 t}\left(I_1 + jQ_1 + Ae^{j\omega_{RF_1}t}\right) \tag{4}$$

As intended, we have the data propagating at a frequency ω_1 while the pure tone has been shifted to $\omega_1 + \omega_{RF_1}$.

A perfect detection after a lossless and noiseless transmission yields to a current like:

$$\begin{aligned} I_{det_1} \propto |E_{out_1}|^2 =& I_1^2 + Q_1^2 + A^2 \\ &+2A\left(I_1\cos(\omega_{RF_1}t) + Q_1\sin(\omega_{RF_1}t)\right) \end{aligned} \tag{5}$$

From there, the I and Q data can be recovered by multiplying by $\cos(\omega_{RF_1}t)$ and $\sin(\omega_{RF_1}t)$ respectively followed by a low pass filter. (See fig 1,Details are to be found in Appendix [2])

The second part of the system will use the incoming field to send the uplink data. To do so, the second nMZM will be used with applied tensions to each branch:

$$\begin{aligned} V_{RFA} &= I_2\cos(\omega_{RF_2}t) - Q_2\sin(\omega_{RF_2}t) \\ V_{RFB} &= I_2\sin(\omega_{RF_2}t) + Q_2\cos(\omega_{RF_2}t) \end{aligned} \tag{6}$$

The resulting transmitted field becomes (using (4)):

$$\begin{aligned} E_{out_2} &= E_{out_1}\left((I_2 + jQ_2)e^{j\omega_{RF_2}t}\right) \\ &= (I_1 + jQ_1)(I_2 + jQ_2)e^{j(\omega_1 t + \omega_{RF_2}t)} \\ &+ A(I_2 + jQ_2)e^{j(\omega_1 t + \omega_{RF_1}t + \omega_{RF_2}t)} \end{aligned} \tag{7}$$

One can easily identify the data of interest at $\omega_1 + \omega_{RF_1} + \omega_{RF_2}$ while an other unusable package travels at $\omega_1 + \omega_{RF_2}$. This successfully allows a propagation within the same fiber without confusion at the detection between the back-scattered light and the actual information.

Adding up a pure tone for the detection results, after habile manipulation, in obtaining a signal with frequency components in 0, f_{RF1}, f_{RF2} & $f_{RF1} + f_{RF2}$ (see Appendix [3] for resolution details). From there, through

a similar process as in the first detection, one can isolate the I and Q data.

As a proposal for a new telecommunications system, our focus is to maintain the cost as low as possible, and so reduce the needed power. To do so, the calculation of the Optimal Carrier to Signal Ratio (OCSR) will what relation should be maintained for maximizing the RF power detected with a fixed optical power at the photodetector input. We will now study the case of the downlink:

Starting from a more realistic representation of the response of a nMZM and setting the bias voltages at V_π, with the same applied tensions as previously, one can isolate the output field component carrying each part of the signal in the form:

Component carrying the I information:

$$-\frac{\pi}{2}aIJ_0(\frac{\pi}{2}A) - 2J_1(\frac{\pi}{2}A)\cos(\omega t) \tag{8}$$

Component carrying the Q information:

$$-j\frac{\pi}{2}aQJ_0(\frac{\pi}{2}A) - j2J_1(\frac{\pi}{2}A)\sin(\omega t) \tag{9}$$

The ratio between signal and carrier can then be expressed as:

$$OCSR \approx \left(\frac{2J_1(\frac{\pi}{2}A)}{\frac{\pi}{2}aJ_0(\frac{\pi}{2}A)}\right)^2 \tag{10}$$

(Detailed reasonning to be found in Appendix [4]).

The field can then be writen in function of m (with m s.t. $OCSR = \frac{1}{m^2}$:

$$E_{out} = E_0[1 + m(I + jQ)e^{-j\omega t}] \tag{11}$$

With this formulation, it can be shown that the power of the signal of interest is maximized for $m = \frac{\pi * A}{2V_\pi}$.

B. Data treatment and simulations

This section contains numerical simulations using Matlab of the downlink operation. The code developed will also serve the purpose of generating the data to be loaded into the arbitrary wave generator in our experiment setup. An array of bits was randomly generated and translated into symbols in two different offline arrays (I_1, Q_1), having each symbol 2 bits. Firstly a zero padding was done, and then the signal was interpolated using a square root raised cosine, understanding that it will be applied twice (both transmission as reception filter) to globally end up applying a raised cosine filter (RC). RC filter is used as it has limited bandwidth while allowing us to control the inter symbol interference (ISI). Once the filtering is done for both I_1, Q_1, we add them to their sampled respective carrier (equations 3 & 4), resulting in the electric waveform ready to be generated using the AWG and sent through the system. After passing through the system, a single signal E'_{out1} is photodetected as described in equation 6, and is separated into two demodulated new signals using multipliers, from which we can extract the original data using a low pass filter. Having done that only the reception SSRC filter remains to be applied. Having done so, the data is recovered by downsampling. (All corresponding figures in Appendix 6).

We examined the optical spectrum of the transmitted signal without linear approximations (equation 2), as we want to predict the non-linearity effects and higher harmonics.

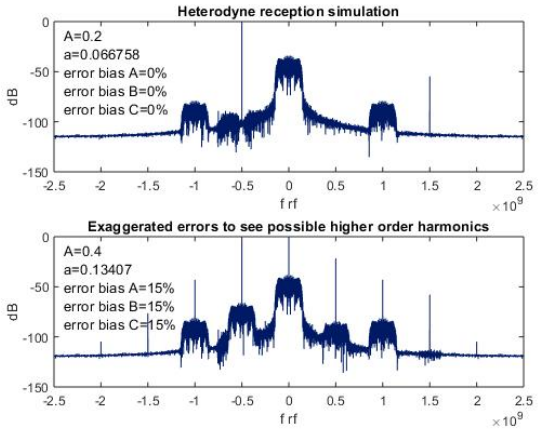

FIG. 3. Simulated optical spectrum for different choices of parameters in the nested MZM

IV. EXPERIMENTAL WORK

A. Setup

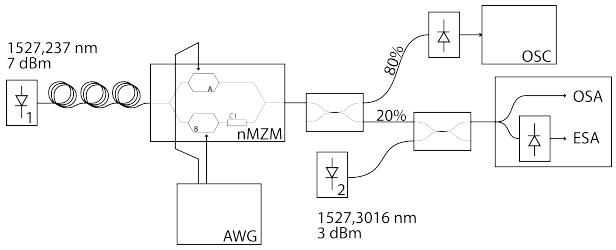

FIG. 4. Experimental setup

Our experimental setup was built to achieve the first part of the system, namely the generation of the signals, modulation of the first laser, transmission and reception. To do so, we used a Tektronix AWG 7052 (Arbitrary Waveform Generator with a maximum sampling rate of 5GS/s), two lasers (an Agilent 8164B Lightwave Measurement System and an Apex AP3350A), a JDS Uniphase nested Mach-Zender modulator, a photodetector, a Hewlett Packard 70004A Display and two power

supplies (Promax FA-851).

The purpose of the second laser is to obtain an optical downconversion of the modulated signal that allows us to visualize the optical spectrum with the resolution of an electrical spectrum analyzer and to distinguish the carrier and sidebands as in Figure 3.We use an asymmetric optical coupler (80/20) so that the detected signal does not suffer significant optical power loss. The second laser set at $1527.3016nm$ and $3dBm$ used for heterodyne detection is then added. This configuration gives us control on the bias drift and allowed us to capture the received signal.

Having the sample rated fixed at it maximum value, we considered a bit rate of $500Mbits/s$ and a RF frequency of $500MHz$. Our equipment allowed us to try and generate up to 2^{11} bits, given that we used 20 samples per symbol, which is a reasonable amount of samples to construct a reliable picture of the carrier and insures the right time window given the bit rate.

As depicted in Figure 4, the first laser set at $1527.237nm$ with a power of $7dBm$ acts as carrier. After a phase control to minimize the insertion losses, it is modulated and shifted as exposed in III A. The biases used to reach the null point were:

	V_{BA}	V_{BB}	V_{BC}
V (V)	0.43	0.80	4.66

B. Results

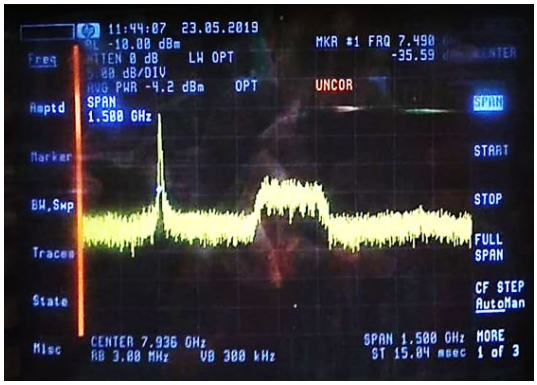

FIG. 5. Spectrum obtained with the Electrical Spectrum Analyzer after the laser heterodyning

The obtained spectrum (Figure 5) shows the expected peak of the carrier shifted $500MHz$ from the characteristic spectrum of the data, as predicted in the simulations in figure 5 taking into account that the higher order harmonics are below the noise contribution and are not observed, while in the following figure 6 where non linearities where intended we can see the mix between the carrier and the data and the higher order harmonics raising due to subtle changes in A and B biases that drive the null point away.

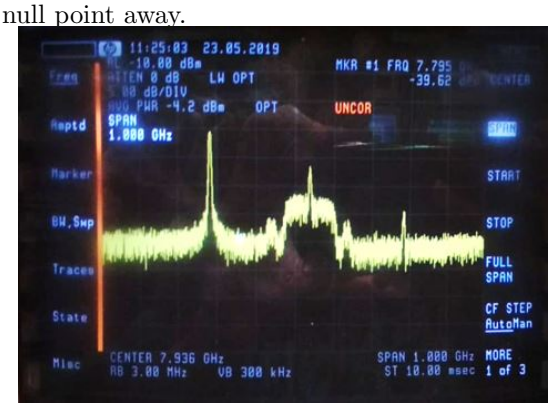

FIG. 6. Non-linearities are observable if the null point is lost

C. Complications

To reach this result, various factors had to be taken into account. First of all, a non ideal Extinction Ratio (described in Appendix [1]) limits the ability to cancel out one of the two carriers that could appear (on the left and on the right of our data). These difficulties to obtain the ideal result depicted in Equation 4 where amplified by the permanent bias drift, and the resulting complexity of polarizing the system at the right values of V_π. This implies that, without the use of an automated bias control one can only ensure the stability for the time of a measurement. Furthermore, to avoid added phases at the electrical level it has revealed imperative to maintain the symmetry of the installation, i.e. using cables of same lengths.

V. CONCLUSIONS

This work established the basis for the examination of feasibility of a full-duplex network access with colourless and source-free optical network unit. It provided a basic analytic frame of the problem, and the first experimental confirmations. It has been seen that the nested Mach Zehnder enables us to simultaneously produce an IQ modulation and a frequency shifting.

The obtention of the expected spectrum opens the door to future research to be done. That is work on data analysis with the correspondent demodulation, phase control and sampling adaptation with study of the BER and then the implementation of the system described for the uplink.

VI. REFERENCES

[1] Nurul Syafiqah Yap Abdullah (2006) *The effect of longitudinal electric field on pockel cell of lithium niobate (LiNbO3) crystal.*

Appendix 1: Models of the Mach-Zender

Model of the single Push-Pull MZM

In the push-pull we obtain a division of the input field and then application of a potential on each branch. The coefficient κ defines the proportion of incoming power in each branch, and would ideally be 1.

$$E_{out} = \frac{E_{Max}}{1+\kappa}\left[e^{+j\theta/2} + \kappa e^{-j\theta/2}\right] \tag{1}$$

With:

$$\theta(t) = \frac{\pi}{V_\pi}V_T(t) = \frac{\pi}{V_\pi}(V_B + V(t)) \tag{2}$$

One can rewrite the outgoing field as:

$$E_{out} = E_{Max}\left[\cos(\frac{\theta(t)}{2}) + j\frac{1}{\sqrt{E_R}}\sin(\frac{\theta(t)}{2})\right] \tag{3}$$

With the defined Extinction Ratio as:

$$E_R = \frac{P_{max}}{P_{min}} = \left|\frac{E_{max}}{E_{min}}\right|^2 = \left|\frac{1+\kappa}{1-\kappa}\right|^2 \tag{4}$$

Model of the single Dual-Drive MZM

In the case of the dual-drive, a tension is applied to only one of the branches. In this case:

$$\begin{aligned} E_{out} &= \frac{E_{Max}}{1+\kappa}\left[1 + \kappa e^{-j\theta_B}\right] \\ &= E_{Max}\left[\cos(\theta_B(t)) + j\frac{\kappa}{1+\kappa}\sin(\theta_B(t))\right] \end{aligned} \tag{5}$$

Model of the nested Mach-Zender

Putting together the three Mach-Zenders:

$$\begin{aligned} E_{out} &= \frac{E_{Max}}{1+\kappa_3}\left[E_{out_1} + \kappa_3 E_{out_2} e^{-j\theta_{B3}}\right] \\ &= E_{Max}\left[\cos(\theta_B(t)) + j\frac{\kappa}{1+\kappa}\sin(\theta_B(t))\right] \end{aligned} \tag{6}$$

Appendix 2: Linear model of the downlink

We will first present the simplified resulting fields obtained at the outphut of the first nMZM, the data after the first detection (downlink), the output field of the second nMZM and the final obtained data of the uplink. To do so we will consider an ideal MZM splitting the input field in 2 (i.e. $\kappa = 1$) in the linear approximation of the senoidal response.

First nMZM

Input field created by the laser:

$$E_{in} = e^{j\omega_1 t} \tag{7}$$

Applied tensions to each MZ:

$$V_{RFA} = I_1 + A\cos(\omega_{RF_1} t) \tag{8}$$

$$V_{RFB} = Q_1 + A\sin(\omega_{RF_1} t) \tag{9}$$

Output field after the nested Mach-Zender modulator:

$$\begin{aligned} E_{out} &= e^{j\omega_1 t}\left(I_1 + A\cos(\omega_{RF_1} t) + jQ_1 + jA\sin(\omega_{RF_1} t)\right) \\ &= e^{j\omega_1 t}\left(I_1 + jQ_1 + Ae^{j\omega_{RF_1} t}\right) \end{aligned} \tag{10}$$

First detector

Obtained measure by the first detector in the case of an ideal transmission:

$$\begin{aligned} I_{det_1} &\propto \left|e^{j\omega_1 t}\left(I_1 + jQ_1 + Ae^{j\omega_{RF_1} t}\right)\right|^2 \\ &= \left|I_1 + jQ_1 + Ae^{j\omega_{RF_1} t}\right|^2 \\ &= \left|I_1 + jQ_1 + A\cos(\omega_{RF_1} t) + jA\sin(\omega_{RF_1} t)\right|^2 \\ &= \left(I_1 + A\cos(\omega_{RF_1} t)\right)^2 + \left(Q_1 + A\sin(\omega_{RF_1} t)\right)^2 \\ &= I_1^2 + A^2\cos^2(\omega_{RF_1} t) + 2I_1 A\cos(\omega_{RF_1} t) + Q_1^2 + A^2\sin^2(\omega_{RF_1} t) + 2Q_1 A\sin(\omega_{RF_1} t) \\ &= I_1^2 + Q_1^2 + A^2 + 2A\left(I_1\cos(\omega_{RF_1} t) + Q_1\sin(\omega_{RF_1} t)\right) \end{aligned} \tag{11}$$

First demodulation

Isolating the I information by multiplying by $\cos(\omega_{RF_1} t)$

$$\begin{aligned} &= (I_1^2 + Q_1^2 + A^2)\cos(\omega_{RF_1} t) + 2AI_1\cos^2(\omega_{RF_1} t) + 2AQ_1\sin(\omega_{RF_1} t)\cos(\omega_{RF_1} t) \\ &= AI_1 + (I_1^2 + Q_1^2 + A^2)\cos(\omega_{RF_1} t) + AI_1\cos(2\omega_{RF_1} t) + AQ_1\sin(2\omega_{RF_1} t) \end{aligned} \tag{12}$$

Isolating the Q information by multiplying by $\sin(\omega_{RF_1} t)$

$$\begin{aligned} &= (I_1^2 + Q_1^2 + A^2)\sin(\omega_{RF_1} t) + 2AI_1\cos(\omega_{RF_1} t)\sin(\omega_{RF_1} t) + 2AQ_1\sin^2(\omega_{RF_1} t) \\ &= AQ_1 + (I_1^2 + Q_1^2 + A^2)\sin(\omega_{RF_1} t) + AI_1\sin(2\omega_{RF_1} t) + AQ_1\cos(2\omega_{RF_1} t) \end{aligned} \tag{13}$$

Appendix 3: Linear model of the uplink

Second nMZM
Applied tensions to each MZ:

$$V_{RFA} = I_2 \cos(\omega_{RF_2} t) - Q_2 \sin(\omega_{RF_2} t) \tag{14}$$

$$V_{RFB} = I_2 \sin(\omega_{RF_2} t) + Q_2 \cos(\omega_{RF_2} t) \tag{15}$$

Effect of the second NMZM on the field:

$$\begin{aligned} E_{out_2} &= E_{in_2} \left(V_{RFA} + j V_{RFB} \right) \\ &= E_{in_2} \left(I_2 \cos(\omega_{RF_2} t) - Q_2 \sin(\omega_{RF_2} t) + j \left(I_2 \sin(\omega_{RF_2} t) + Q_2 \cos(\omega_{RF_2} t) \right) \right) \\ &= E_{in_2} \left(I_2 \left(\cos(\omega_{RF_2} t) + j \sin(\omega_{RF_2} t) \right) + Q_2 \left(-\sin(\omega_{RF_2} t) + j \cos(\omega_{RF_2} t) \right) \right) \\ &= E_{in_2} \left(I_2 e^{j\omega_{RF_2} t} + j Q_2 e^{j\omega_{RF_2} t} \right) \\ &= E_{in_2} \left((I_2 + j Q_2) e^{j\omega_{RF_2} t} \right) \end{aligned} \tag{16}$$

Using Equation (10)

$$\begin{aligned} E_{out_2} &= e^{j\omega_1 t} \left[I_1 + j Q_1 + A e^{j\omega_{RF_1} t} \right] \left((I_2 + j Q_2) e^{j\omega_{RF_2} t} \right) \\ &= (I_2 + j Q_2) e^{j\omega_{RF_2} t} e^{j\omega_1 t} (I_1 + j Q_1) + A (I_2 + j Q_2) e^{j\omega_{RF_2} t} e^{j\omega_{RF_1} t} e^{j\omega_1 t} \\ &= (I_1 + j Q_1)(I_2 + j Q_2) e^{j(\omega_1 t + \omega_{RF_2} t)} + A (I_2 + j Q_2) e^{j(\omega_1 t + \omega_{RF_1} t + \omega_{RF_2} t)} \end{aligned} \tag{17}$$

Second detector
Adding a pure tone before detection

$$\begin{aligned} E_{det} &= E_{out_2} + e^{j\omega_4 t} \\ &= (I_1 + j Q_1)(I_2 + j Q_2) e^{j(\omega_1 t + \omega_{RF_2} t)} + A (I_2 + j Q_2) e^{j(\omega_1 t + \omega_{RF_1} t + \omega_{RF_2} t)} + e^{j\omega_4 t} \end{aligned} \tag{18}$$

Signal obtained by the second detector

$$\begin{aligned} I_{det_2} &\propto |E_{det}|^2 \\ &= \left| (I_1 + j Q_1)(I_2 + j Q_2) e^{j(\omega_1 t + \omega_{RF_2} t)} + A (I_2 + j Q_2) e^{j(\omega_1 t + \omega_{RF_1} t + \omega_{RF_2} t)} + e^{j\omega_4 t} \right|^2 \\ &= \left| (I_1 I_2 - Q_1 Q_2 + j I_1 Q_2 + j Q_1 I_2) e^{j(\omega_1 t + \omega_{RF_2} t)} + A (I_2 + j Q_2) e^{j(\omega_1 t + \omega_{RF_1} t + \omega_{RF_2} t)} + e^{j\omega_4 t} \right|^2 \\ &= \left((I_1 I_2 - Q_1 Q_2 + j(I_1 Q_2 + Q_1 I_2)) e^{j(\omega_1 t + \omega_{RF_2} t)} + A (I_2 + j Q_2) e^{j(\omega_1 t + \omega_{RF_1} t + \omega_{RF_2} t)} + e^{j\omega_4 t} \right) \\ &\cdot \left((I_1 I_2 - Q_1 Q_2 - j(I_1 Q_2 + Q_1 I_2)) e^{-j(\omega_1 t + \omega_{RF_2} t)} + A (I_2 - j Q_2) e^{-j(\omega_1 t + \omega_{RF_1} t + \omega_{RF_2} t)} + e^{-j\omega_4 t} \right) \\ &= (I_1 I_2 - Q_1 Q_2)^2 + (I_1 Q_2 + Q_1 I_2)^2 + A^2 (I_2^2 + j Q_2^2) + 1 \\ &+ A (I_2 - j Q_2)(I_1 I_2 - Q_1 Q_2 + j(I_1 Q_2 + Q_1 I_2)) e^{-j\omega_{RF_1} t} + (I_1 I_2 - Q_1 Q_2 + j(I_1 Q_2 + Q_1 I_2)) e^{j(\omega_1 t + \omega_{RF_2} t - \omega_4 t)} \\ &+ A (I_2 + j Q_2)(I_1 I_2 - Q_1 Q_2 - j(I_1 Q_2 + Q_1 I_2)) e^{j\omega_{RF_1} t} + (I_1 I_2 - Q_1 Q_2 - j(I_1 Q_2 + Q_1 I_2)) e^{-j(\omega_1 t + \omega_{RF_2} t - \omega_4 t)} \\ &+ A (I_2 + j Q_2) e^{j(\omega_1 t + \omega_{RF_1} t + \omega_{RF_2} t - \omega_4 t)} + A (I_2 - j Q_2) e^{-j(\omega_1 t + \omega_{RF_1} t + \omega_{RF_2} t - \omega_4 t)} \end{aligned} \tag{19}$$

Using the same laser for detection as in the initial emition: $\omega_4 = \omega_1$:

$$
\begin{aligned}
I_{det_2} &\propto |E_{det}|^2 \\
&= (I_1I_2 - Q_1Q_2)^2 + (I_1Q_2 + Q_1I_2)^2 + A^2(I_2^2 + jQ_2^2) + 1 \\
&+ A(I_2 - jQ_2)(I_1I_2 - Q_1Q_2 + j(I_1Q_2 + Q_1I_2))e^{-j\omega_{RF_1}t} + (I_1I_2 - Q_1Q_2 + j(I_1Q_2 + Q_1I_2))e^{j\omega_{RF_2}t} \\
&+ A(I_2 + jQ_2)(I_1I_2 - Q_1Q_2 - j(I_1Q_2 + Q_1I_2))e^{j\omega_{RF_1}t} + (I_1I_2 - Q_1Q_2 - j(I_1Q_2 + Q_1I_2))e^{-j\omega_{RF_2}t} \\
&+ A(I_2 + jQ_2)e^{j(\omega_{RF_1}+\omega_{RF_2})t} + A(I_2 - jQ_2)e^{-j(\omega_{RF_1}+\omega_{RF_2})t} \\
&= (I_1I_2 - Q_1Q_2)^2 + (I_1Q_2 + Q_1I_2)^2 + A^2(I_2^2 + jQ_2^2) + 1 \\
&+ A(I_2 - jQ_2)(I_1I_2 - Q_1Q_2 + j(I_1Q_2 + Q_1I_2))e^{-j\omega_{RF_1}t} \\
&+ A(I_2 + jQ_2)(I_1I_2 - Q_1Q_2 - j(I_1Q_2 + Q_1I_2))e^{j\omega_{RF_1}t} \\
&+ (I_1I_2 - Q_1Q_2 + j(I_1Q_2 + Q_1I_2))e^{j\omega_{RF_2}t} \\
&+ (I_1I_2 - Q_1Q_2 - j(I_1Q_2 + Q_1I_2))e^{-j\omega_{RF_2}t} \\
&+ A(I_2 + jQ_2)e^{j(\omega_{RF_1}+\omega_{RF_2})t} + A(I_2 - jQ_2)e^{-j(\omega_{RF_1}+\omega_{RF_2})t} \\
&= (I_1I_2 - Q_1Q_2)^2 + (I_1Q_2 + Q_1I_2)^2 + A^2(I_2^2 + jQ_2^2) + 1 \\
&+ A\left[I_2(I_1I_2 - Q_1Q_2) + Q_2(I_1Q_2 + Q_1I_2))\right]e^{-j\omega_{RF_1}t} - jA\left[Q_2(I_1I_2 - Q_1Q_2) - I_2(I_1Q_2 + Q_1I_2)\right]e^{-j\omega_{RF_1}t} \\
&+ A\left[I_2(I_1I_2 - Q_1Q_2) + Q_2(I_1Q_2 + Q_1I_2))\right]e^{j\omega_{RF_1}t} - jA\left[-Q_2(I_1I_2 - Q_1Q_2) + I_2(I_1Q_2 + Q_1I_2)\right]e^{j\omega_{RF_1}t} \\
&+ (I_1I_2 - Q_1Q_2 + j(I_1Q_2 + Q_1I_2))e^{j\omega_{RF_2}t} \\
&+ (I_1I_2 - Q_1Q_2 - j(I_1Q_2 + Q_1I_2))e^{-j\omega_{RF_2}t} \\
&+ A(I_2 + jQ_2)e^{j(\omega_{RF_1}+\omega_{RF_2})t} + A(I_2 - jQ_2)e^{-j(\omega_{RF_1}+\omega_{RF_2})t}
\end{aligned}
\tag{20}
$$

Using the definitions of sin and cos functions, on can rewrite:

$$
\begin{aligned}
I_{det_2} \propto\ & (I_1I_2 - Q_1Q_2)^2 + (I_1Q_2 + Q_1I_2)^2 + A^2(I_2^2 + jQ_2^2) + 1 \\
&+ 2A\left[I_2(I_1I_2 - Q_1Q_2) + Q_2(I_1Q_2 + Q_1I_2))\right]\cos(\omega_{RF_1}t) \\
&- 2A\left[Q_2(I_1I_2 - Q_1Q_2) - I_2(I_1Q_2 + Q_1I_2)\right]\sin(\omega_{RF_1}t) \\
&+ 2(I_1I_2 - Q_1Q_2)\cos(\omega_{RF_2}t) - 2(I_1Q_2 + Q_1I_2))\sin(\omega_{RF_2}t) \\
&+ 2AI_2\cos((\omega_{RF_1} + \omega_{RF_2})t) - 2AQ_2\sin((\omega_{RF_1} + \omega_{RF_2})t)
\end{aligned}
\tag{21}
$$

Isolating the I information by multiplying by $\cos((\omega_{RF_1} + \omega_{RF_2})t)$

$$
\begin{aligned}
&= \Big[(I_1I_2 - Q_1Q_2)^2 + (I_1Q_2 + Q_1I_2)^2 + A^2(I_2^2 + jQ_2^2) + 1\Big]\cos((\omega_{RF_1} + \omega_{RF_2})t) \\
&+ 2A\Big[I_2(I_1I_2 - Q_1Q_2) + Q_2(I_1Q_2 + Q_1I_2))\Big]\cos(\omega_{RF_1}t)\cos((\omega_{RF_1} + \omega_{RF_2})t) \\
&- 2A\Big[Q_2(I_1I_2 - Q_1Q_2) - I_2(I_1Q_2 + Q_1I_2)\Big]\sin(\omega_{RF_1}t)\cos((\omega_{RF_1} + \omega_{RF_2})t) \\
&+ 2(I_1I_2 - Q_1Q_2)\cos(\omega_{RF_2}t)\cos((\omega_{RF_1} + \omega_{RF_2})t) - 2(I_1Q_2 + Q_1I_2))\sin(\omega_{RF_2}t)\cos((\omega_{RF_1} + \omega_{RF_2})t) \\
&+ 2AI_2\cos^2((\omega_{RF_1} + \omega_{RF_2})t) - 2AQ_2\sin((\omega_{RF_1} + \omega_{RF_2})t)\cos((\omega_{RF_1} + \omega_{RF_2})t) \\
&= \Big[(I_1I_2 - Q_1Q_2)^2 + (I_1Q_2 + Q_1I_2)^2 + A^2(I_2^2 + jQ_2^2) + 1\Big]\cos((\omega_{RF_1} + \omega_{RF_2})t) \\
&+ A\Big[I_2(I_1I_2 - Q_1Q_2) + Q_2(I_1Q_2 + Q_1I_2))\Big]\Big(\cos((2\omega_{RF_1} + \omega_{RF_2})t) + \cos(\omega_{RF_2}t)\Big) \\
&- A\Big[Q_2(I_1I_2 - Q_1Q_2) - I_2(I_1Q_2 + Q_1I_2)\Big]\Big(\sin((2\omega_{RF_1} + \omega_{RF_2})t) - \sin(\omega_{RF_2}t)\Big) \\
&+ (I_1I_2 - Q_1Q_2)\Big(\cos((\omega_{RF_1} + 2\omega_{RF_2})t) + \cos(\omega_{RF_1}t)\Big) \\
&- (I_1Q_2 + Q_1I_2))\Big(\sin((\omega_{RF_1} + 2\omega_{RF_2})t) - \sin(\omega_{RF_1}t)\Big) \\
&- AQ_2\sin(2(\omega_{RF_1} + \omega_{RF_2})t) + AI_2\cos(2(\omega_{RF_1} + \omega_{RF_2})t) + AI_2
\end{aligned}
\tag{22}
$$

From this last equation it is obvious one can recover the I data using a low-pass filter.
Isolating the Q information by multiplying by $\sin((\omega_{RF_1} + \omega_{RF_2})t)$

$$
\begin{aligned}
&= \Big[(I_1I_2 - Q_1Q_2)^2 + (I_1Q_2 + Q_1I_2)^2 + A^2(I_2^2 + jQ_2^2) + 1\Big] \sin((\omega_{RF_1} + \omega_{RF_2})t) \\
&+ 2A\Big[I_2(I_1I_2 - Q_1Q_2) + Q_2(I_1Q_2 + Q_1I_2))\Big] \cos(\omega_{RF_1}t) \sin((\omega_{RF_1} + \omega_{RF_2})t) \\
&- 2A\Big[Q_2(I_1I_2 - Q_1Q_2) - I_2(I_1Q_2 + Q_1I_2)\Big] \sin(\omega_{RF_1}t) \sin((\omega_{RF_1} + \omega_{RF_2})t) \\
&+ 2(I_1I_2 - Q_1Q_2) \cos(\omega_{RF_2}t) \sin((\omega_{RF_1} + \omega_{RF_2})t) - 2(I_1Q_2 + Q_1I_2)) \sin(\omega_{RF_2}t) \sin((\omega_{RF_1} + \omega_{RF_2})t) \\
&+ 2AI_2 \cos((\omega_{RF_1} + \omega_{RF_2})t) \sin((\omega_{RF_1} + \omega_{RF_2})t) - 2AQ_2 \sin^2((\omega_{RF_1} + \omega_{RF_2})t) \\
&= \Big[(I_1I_2 - Q_1Q_2)^2 + (I_1Q_2 + Q_1I_2)^2 + A^2(I_2^2 + jQ_2^2) + 1\Big] \sin((\omega_{RF_1} + \omega_{RF_2})t) \\
&+ A\Big[I_2(I_1I_2 - Q_1Q_2) + Q_2(I_1Q_2 + Q_1I_2))\Big] \Big(\sin((2\omega_{RF_1} + \omega_{RF_2})t) - \sin(-\omega_{RF_2}t)\Big) \\
&- A\Big[Q_2(I_1I_2 - Q_1Q_2) - I_2(I_1Q_2 + Q_1I_2)\Big] \Big(- \cos((2\omega_{RF_1} + \omega_{RF_2})t) + \cos(\omega_{RF_2}t)\Big) \\
&+ (I_1I_2 - Q_1Q_2)\Big(\sin((\omega_{RF_1} + 2\omega_{RF_2})t) - \sin(-\omega_{RF_1}t)\Big) \\
&- (I_1Q_2 + Q_1I_2))\Big(- \cos((\omega_{RF_1} + 2\omega_{RF_2})t) + \sin(\omega_{RF_1}t)\Big) \\
&+ AI_2 \sin(2(\omega_{RF_1} + \omega_{RF_2})t) + AQ_2 \cos(2(\omega_{RF_1} + \omega_{RF_2})t) - AQ_2
\end{aligned}
\tag{23}
$$

Appendix 4: Ideal calculation of the Optimal Carrier to Signal Ratio

With Transfer function

$$\begin{aligned} E_{out} &= \frac{E_{in}}{2}\left[\frac{1}{2}[e^{j\frac{\pi}{2V_\pi}\hat{V}_1}+e^{-j\frac{\pi}{2V_\pi}\hat{V}_1}]+\frac{j}{2}[e^{j\frac{\pi}{2V_\pi}\hat{V}_2}+e^{-j\frac{\pi}{2V_\pi}\hat{V}_2}]\right] \\ &= \frac{E_i n}{2}\left[\cos\frac{\pi}{2V_\pi}\hat{V}_1+cos\frac{\pi}{2V_\pi}\hat{V}_2\right] \end{aligned} \tag{24}$$

Using:

$$\begin{cases} \hat{V}_i = V_{Bi}+V_i \\ V_1 = aI + A\cos(\omega t) \\ V_2 = aQ + A\sin(\omega t) \\ V_{Bi} = V_\pi \end{cases} \tag{25}$$

$$\begin{aligned} E_{out} &= \frac{E_{in}}{2}\left[\cos(\frac{\pi}{2}+\frac{\pi}{2V_\pi}(aI+A\cos(\omega t)))+j\cos(\frac{\pi}{2}+\frac{\pi}{2V_\pi}(aQ+A\sin(\omega t)))\right] \\ &= \frac{E_{in}}{2}\left[-\sin(\frac{\pi}{2V_\pi}(aI+A\cos(\omega t)))-j\sin(\frac{\pi}{2V_\pi}(aQ+A\sin(\omega t)))\right] \end{aligned} \tag{26}$$

Considering $V_\pi = 1$
Jacobi-Anger relations:

$$\cos(z\cos\theta) \equiv J_0(z)+2\sum_{n=1}^{\infty}(-1)^n J_{2n}(z)\cos(2n\theta) \tag{27}$$

$$\sin(z\cos\theta) \equiv -2\sum_{n=1}^{\infty}(-1)^n J_{2n-1}(z)\cos((2n-1)\theta) \tag{28}$$

$$\cos(z\sin\theta) \equiv J_0(z)+2\sum_{n=1}^{\infty}J_{2n}(z)\cos(2n\theta) \tag{29}$$

$$\sin(z\sin\theta) \equiv 2\sum_{n=1}^{\infty}J_{2n-1}(z)\sin((2n-1)\theta) \tag{30}$$

Component carrying the I information (using (27) and (28)):

$$\begin{aligned} &-\sin(\frac{\pi}{2}(aI+A\cos(\omega t))) \\ =&-\sin(\frac{\pi}{2}aI)\cos(\frac{\pi}{2}A\cos(\omega t))-\cos(\frac{\pi}{2}aI)\sin(\frac{\pi}{2}A\cos(\omega t)) \\ \approx&-\frac{\pi}{2}aI\cos(\frac{\pi}{2}A\cos(\omega t))-\sin(\frac{\pi}{2}A\cos(\omega t)) \\ \approx&-\frac{\pi}{2}aIJ_0(\frac{\pi}{2}A)-2J_1(\frac{\pi}{2}A)\cos(\omega t) \end{aligned} \tag{31}$$

Component carrying the Q information (using (29) and (30)):

$$\begin{aligned} &-j\sin(\frac{\pi}{2}(aQ+A\sin(\omega t))) \\ =&-j\sin(\frac{\pi}{2}aQ)\cos(\frac{\pi}{2}A\sin(\omega t))-j\cos(\frac{\pi}{2}aQ)\sin(\frac{\pi}{2}A\sin(\omega t)) \\ \approx&-j\frac{\pi}{2}aQ\cos(\frac{\pi}{2}A\sin(\omega t))-j\sin(\frac{\pi}{2}A\sin(\omega t)) \\ \approx&-j\frac{\pi}{2}aQJ_0(\frac{\pi}{2}A)-j2J_1(\frac{\pi}{2}A)\sin(\omega t) \end{aligned} \tag{32}$$

Carrier: $\sim 2J_1(\frac{\pi}{2}A) \approx \frac{\pi}{2}A$
Signal: $\sim \frac{\pi}{2}aJ_0(\frac{\pi}{2}A) \approx \frac{\pi}{2}a$
Optical Carrier to Signal (Sideband) Ratio:

$$OCSR \approx \left(\frac{2J_1(\frac{\pi}{2}A)}{\frac{\pi}{2}aJ_0(\frac{\pi}{2}A)}\right)^2 \approx \left(\frac{A}{a}\right)^2 \tag{33}$$

Rewriting the output field using (31) and (32):

$$\begin{aligned} E_{out} &\approx \frac{E_{in}}{2}\left[-\frac{\pi}{2}aIJ_0(\frac{\pi}{2}A) - 2J_1(\frac{\pi}{2}A)\cos(\omega t) - j\frac{\pi}{2}aQJ_0(\frac{\pi}{2}A) - j2J_1(\frac{\pi}{2}A)\sin(\omega t)\right] \\ &= \frac{E_{in}}{2}\left[-\frac{\pi}{2}aJ_0(\frac{\pi}{2}A)(I+jQ) - 2J_1(\frac{\pi}{2}A)[\cos(\omega t) + j\sin(\omega t)]\right] \\ &= -\frac{E_{in}}{2}\left[\frac{\pi}{2}aJ_0(\frac{\pi}{2}A)(I+jQ) + 2J_1(\frac{\pi}{2}A)e^{j\omega t}\right] \\ &= -\frac{E_{in}}{2}2J_1(\frac{\pi}{2}A)e^{j\omega t}\left[1 + \frac{\frac{\pi}{2}aJ_0(\frac{\pi}{2}A)}{2J_1(\frac{\pi}{2}A)}(I+jQ)e^{-j\omega t}\right] \end{aligned} \tag{34}$$

With

$$m = \frac{\frac{\pi}{2}aJ_0(\frac{\pi}{2}A)}{2J_1(\frac{\pi}{2}A)} \tag{35}$$

Finding the optimal value for m:
From (34) and (35):

$$E_{out} \approx -E_{in}(\frac{\pi}{2}A)e^{j\omega t}[1 + m(I+jQ)e^{-j\omega t}] \tag{36}$$

We want to optimize the power of our signal:

$$\begin{aligned} P_{out} = P_T &\propto |E_{out}|^2 \\ &\approx |E_{in}|^2(\frac{\pi}{2}A)^2|1 + m(I+jQ)e^{-j\omega t}|^2 \\ &= |E_{in}|^2(\frac{\pi}{2}A)^2(1 + m(I+jQ)e^{-j\omega t})(1 + m(I-jQ)e^{j\omega t}) \\ &= |E_{in}|^2(\frac{\pi}{2}A)^2\left[1 + m^2(I^2+Q^2) + m(I+jQ)e^{-j\omega t} + m(I-jQ)e^{j\omega t}\right] \\ &= |E_{in}|^2(\frac{\pi}{2}A)^2\left[1 + m^2(I^2+Q^2) + mI(e^{j\omega t}) + e^{-j\omega t}) - jmQ(e^{j\omega t} - e^{-j\omega t})\right] \\ &= |E_{in}|^2(\frac{\pi}{2}A)^2\left[1 + m^2(I^2+Q^2) + 2mI\cos(\omega t) + 2mQ\sin(\omega t)\right] \end{aligned} \tag{37}$$

Having the values of I and Q s.t. $\{I, Q\} = \pm 1/\sqrt{2}$:

$$\begin{aligned} \langle P_{out}\rangle &= \langle P_T\rangle \\ &= |E_{in}|^2(\frac{\pi}{2}A)^2\left[1 + m^2(I^2+Q^2)\right] \\ &= |E_{in}|^2(\frac{\pi}{2}A)^2\left[1 + m^2\right] \end{aligned} \tag{38}$$

The current generated by the signal (at the desired frequency) can be obtained by:

$$i_{RF} \propto 2m|E_{in}|^2(\frac{\pi}{2}A)^2 = 2m|E_0|^2 \tag{39}$$

And so the power:

$$P_{RF} \propto i_{RF}^2 = 2P_0^2m^2 \propto m^2P_0^2 \tag{40}$$

Defining:

$$E_0 = E_{in}\frac{\pi}{2}Ae^{j\omega t} \quad \Rightarrow \quad P_0 \propto |E_0|^2 = |E_{in}|^2(\frac{\pi}{2}A)^2 \tag{41}$$

One obtains:

$$P_0 \propto \frac{\langle P_T\rangle}{1+m^2} \tag{42}$$

Using this relation, we can rewrite:

$$P_{RF} \propto m^2 P_0^2 = m^2 \frac{\langle P_T \rangle^2}{(1+m^2)^2} \tag{43}$$

With

$$OCSR = \frac{1}{m^2} \tag{44}$$

One obtains:

$$P_{RF} \propto \langle P_T \rangle^2 \frac{1/OCSR}{(1+1/OCSR)^2} = \langle P_T \rangle^2 \frac{OCSR}{(1+OCSR)^2} \tag{45}$$

Studiing the derivatives to maximize the function

$$\frac{\partial P_{RF}}{\partial OCSR} = \langle P_T \rangle^2 \frac{(1+OCSR)^2 - OCSR(2(1+OCSR))}{(1+OCSR)^4} = \langle P_T \rangle^2 \frac{(1-OCSR)}{(1+OCSR)^3} \tag{46}$$

The ideal situation that allows to maximize the power of the signal of interest is then:

$$\frac{\partial P_{RF}}{\partial OCSR} = 0 \rightarrow OCSR = 1 \rightarrow m = 1 \tag{47}$$

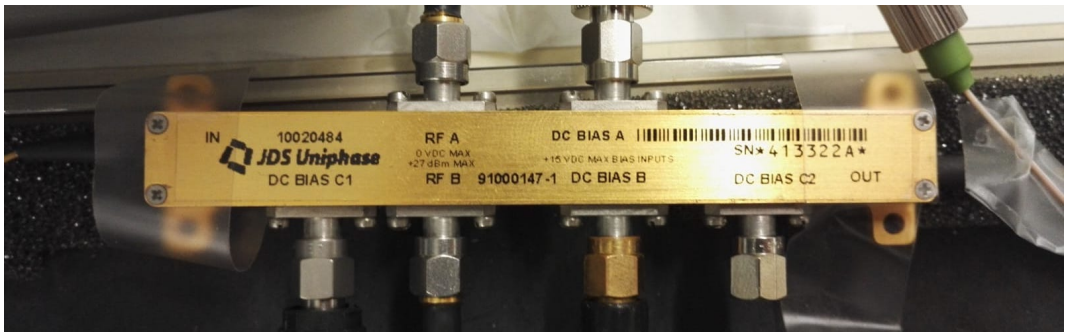

Figure 1: Image of the used device

Appendix 5: Characterization of the Mach Zender Modulator

The used equipment was a JDS Uniphase nested Mach-Zender modulator, allowing to control both branches of the big MZM seperately, and each individual MZM as push-pull. To obtain the value of V_π for each we had to perform various sets of measurements, considering the four entries we had. For this work, we used a Telecom-Test Laser, the JDS Uniphase nested Mach-Zender modulator of interest, some phase correctors, a Promax FA-851 Programmable Power Supply and a Hewlett-Packard photodetector. From know on, we will call A the tension applied to the "DC bias A" entry, B the tension applied to the "DC bias B" entry and so on. The $C2$ entry has been connected to earth, as we want to apply a change of phase of one branch respect to the other, so one of the branches stays untouched.

Various maxima where obtained in specific combination of bias tensions applied: Maxima:

$$\begin{cases} A = 3.29 \\ B = 3.57 \\ C1 = 2 \end{cases} \quad \begin{cases} A = 3.29 \\ B = 8.3 \\ C1 = 6.6 \end{cases} \quad \begin{cases} A = 3.3 \\ B = 3.6 \\ C1 = 12.8 \end{cases} \tag{48}$$

Minima:

$$\begin{cases} A = 3.29 \\ B = 3.57 \\ C1 = 8.0 \end{cases} \quad \begin{cases} A = 3.29 \\ B = 8.3 \\ C1 = 3 \end{cases} \quad \begin{cases} A = 5.33 \\ B = 5.39 \\ C1 = 8 \end{cases} \quad \begin{cases} A = 0.97 \\ B = 0 \\ C1 = 2 \end{cases} \tag{49}$$

These are some pretty exact measurements that have to be used with precaution as we had to face some strong bias drift. The values of tensions to be applied in order to obtain a maximum or a minimum (or any desired position) would vary in time. The repetition of the same measurements showed at best the region in which we had to work, requiring future tuning each time the device would be used in an experiment or even during each experiment. Some more realistic ranges for the maxima would be:

$$\begin{cases} A \in [3.2; 3.3] \\ B \in [3.4; 3.6] \\ C1 \in [0.9; 2] \end{cases} \quad \begin{cases} A \in [2.9; 3.3] \\ B \in [7.7; 8.4] \\ C1 \in [6.6; 7.5] \end{cases} \tag{50}$$

As both transfer functions of the single MZM can be considered senoidal functions, one can interpret these results. Both cosine are of maximum amplitude (± 1) for applied tensions around 3.5 V or 8 V. This let's assume that the null-point is to be found for tensions around 5.5 V, which is coherent with the third minima presented. With these assumptions, $C1$ can be characterized. It creates a phase change of $n\pi$ when being applied tensions around 2 V or 7 V and the periodicity of it explains our third maxima.

Knowing this, we could obtain a maximal power by having both cosines on $+1$ and the phase shift on 0, or having the cosines of opposite sign and adding a π phase. The minima are obtained by adding up the two cosine functions with opposite signs (by having them in opposition of phase or doing that through the big modulator).

We accordingly constructed the estimated transfer functions for the cases $C1 = 2$ and $C1 = 7$ (corresponding to no phase added, or *pi* added) and checked with our measurements to verify the coherence of the interpretations.

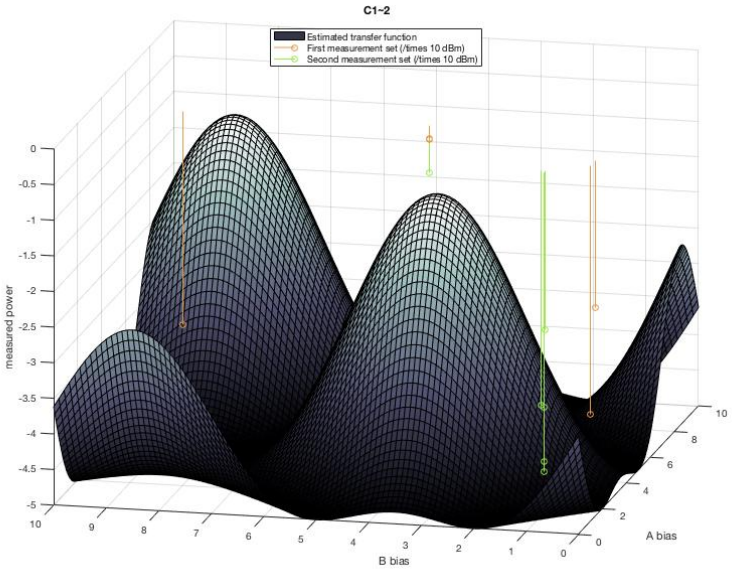

Figure 2: Representation of the estimated transfer function and corresponding measurements for C1=2V

Through this work we could have an idea of the values we would use for the actual experiment. We want a phase added of $\pi/2$ and to have both cosine functions on their null-point. However, it also became clear that we would always need a way to observe our signal at any time, to tune the values while the experiment is going. A applied system would then require an automated bias drift controller, adapting the applied tensions at any time to stay in the working-point.

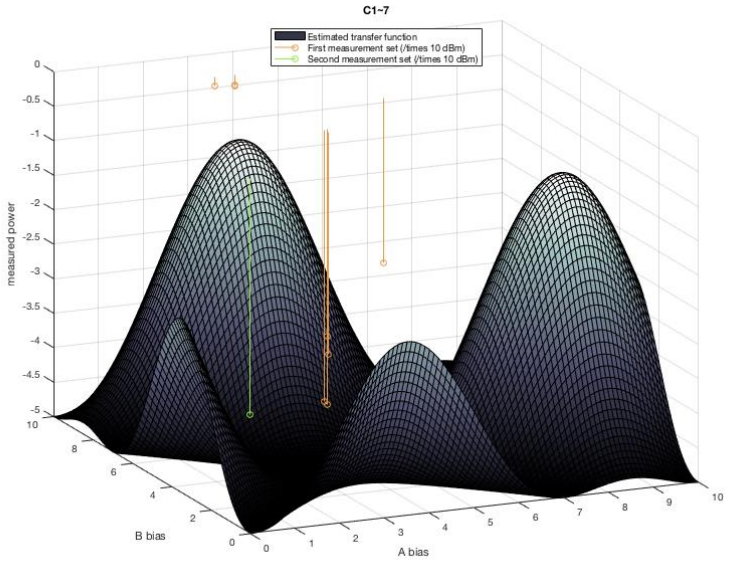

Figure 3: Representation of the estimated transfer function and corresponding measurements for C1=7V

Appendix 6: Numerical generation and demodulation of the signals

Variables

· Number of bits: $Nbits$
· Bit rate: BR $\rightarrow$ Bit time $T_b = 1/BR$
· Bits per symbol: BpS
· Number of symbols: $NS = \frac{Nbits}{BpS}$
· Time window $TW = Nbits \cdot Tb$
· Samples per symbol SpS
· Sample Rate: $SR = SpS \cdot \frac{BR}{BpS}$

Ideal values
· $Nbits = 2^{17}$
· $BR = 1GHz$
· $BpS = 2$
· $TW = 1.3107 \cdot 10^{-4}s$
· $SpS = 2^4$

Experimentally used values
· $Nbits = 2^{11}$
· $BR = 500\ MHz$
· $BpS = 2$
· $TW = 4.096 \cdot 10^{-6}s$
· $SpS = 20$

Data treatment:

Generation of the transmitted signal

As previously stated, in this procedure we use QAM to modulate the transmitted data. Firstly, a bit array is randomly generated and translated into symbols, being each symbol 2 bits.

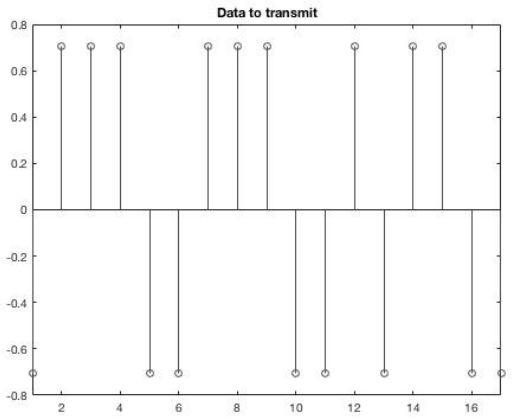

Figure 4: Data generation

Then upsampling was done doing a zero-padding (figure (5)) raised cosine filtering, as it will be needed to reproduce faithfully the carrier. The raised cosine filtering is used as it is a bandwidth limited function which allows us to have zeros in ±Ts, being Ts the time between symbols, and thus cancelling the inter symbol interference.

The total transfer function intended then is

$$H_{RC}(f) = H_{Tx}(f)\Delta H_{channel}(f)\Delta H_{Rx}(f)\Delta H_{equalizer}(f) \tag{51}$$

but considering an ideal channel and so eliminating the equalizer, we can match the transmission and receiving filters $H_{Tx}(f) = H_{Rx}(f) = \sqrt{H_{RC}(f)} = H_{SRRC}(f)$. We used a span of 16 symbols and a rolloff factor o 0.18, and the resulting interpolation normalized resulted in figure 6.

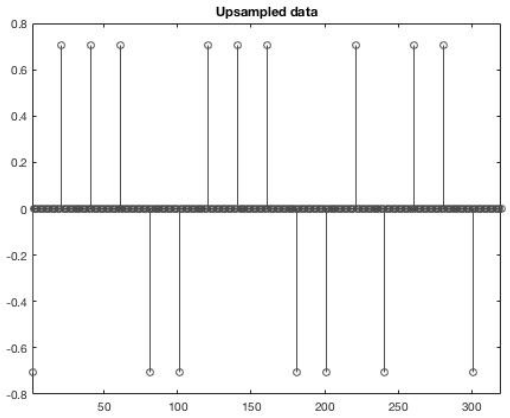

Figure 5: Zero padding

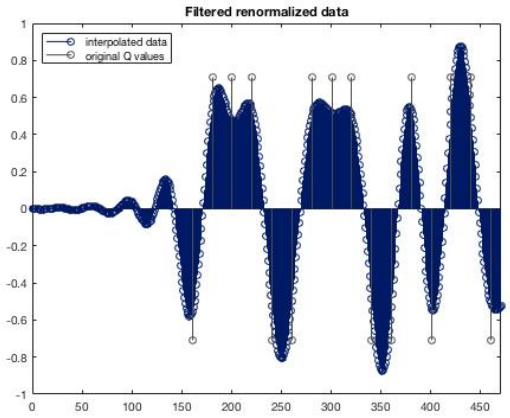

Figure 6: SRRC filtering

But in the previous figures we see how the number of total samples is higher than the original, corresponding to the samples obtained in the multiplications in the convolution where the span of the filter goes further than the limits of our signal, so we trim accordingly (figure 7))

$$\begin{cases} First\,sample = \frac{span\Delta SpS}{2} + 1 - \frac{SpS}{2} \\ \#\,discarded\,last\,samples = \frac{span\Delta SpS}{2} + \frac{SpS}{2} \end{cases} \tag{52}$$

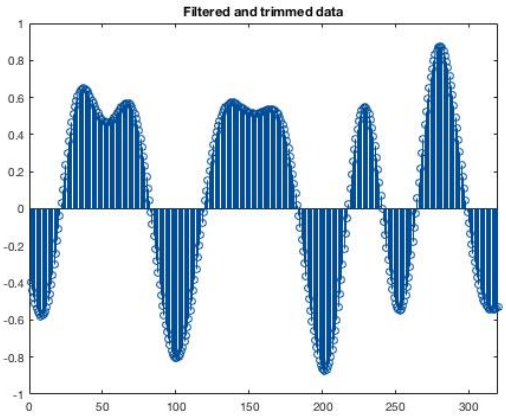

Figure 7: Trimming of the useless queues

Then we can add the carrier function as exposed in the analytical basis, resulting in the following waveform (equations 4 and 5), which is the one that is actually translated from electrical to optical by our MZM result after their summation in equation 6. Figure 8 shows the samples of the first symbols in Q plus the carrier.

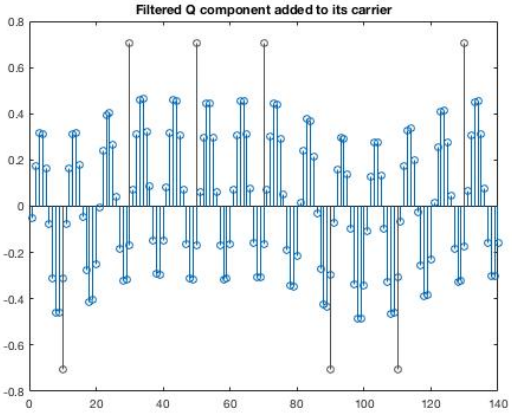

Figure 8: Adding the sampled carrier tone

Demodulation of the received data

Now we present the waveform after the detection using photodetector and multipliers, which corresponds to equation $7\Delta sin(w_{rf}\Delta t)$, as we are presenting the plots corresponding to Q (figure 9)

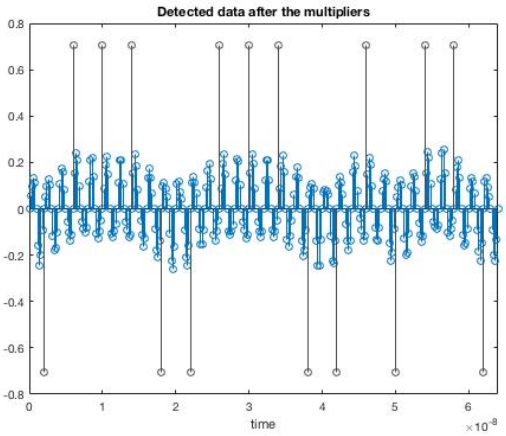

Figure 9: Detection and multiplying

After that we apply the low pass filtering as follows in figure 10

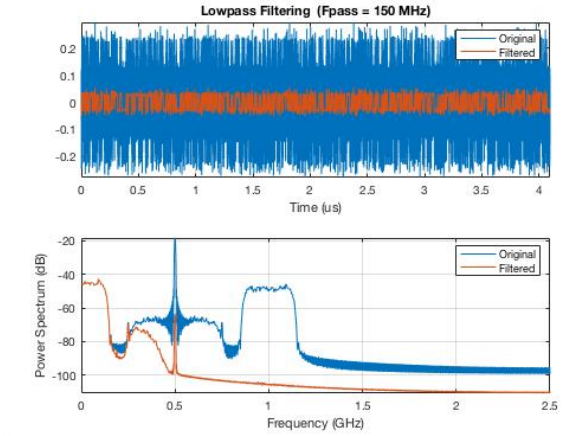

Figure 10: Low pass filtering and frequency spectrum

Resulting in a signal in figure 11

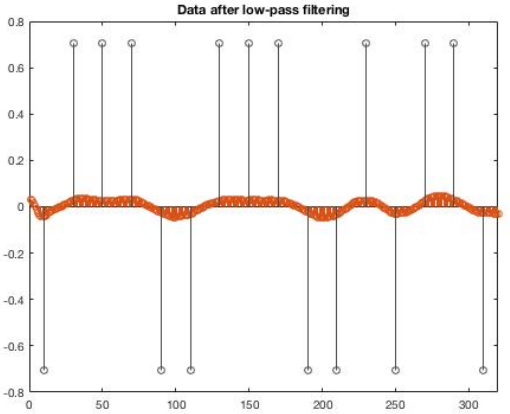

Figure 11: Resulting signal after LP filtering

Now we can apply the receiver filter, which as previously said is srrc to complete the global rc filter (figure 12)

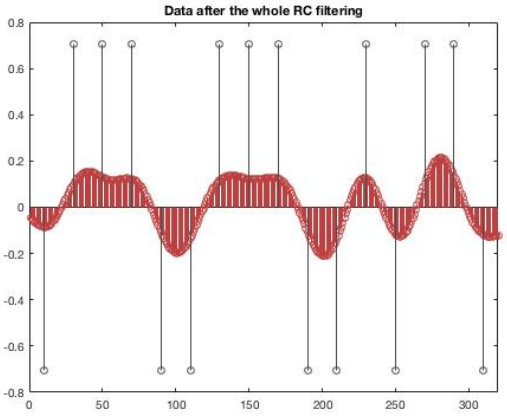

Figure 12: SRRC filtering

And finally we apply a decimation of the same order as our initial interpolation, resultin in 13

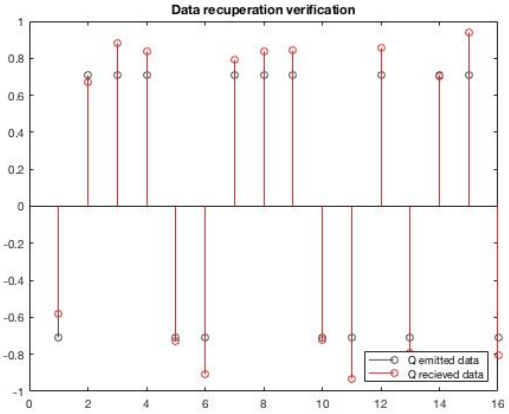

Figure 13: Recuperation of the Q array